Chinese Journal of
POLYMER SCIENCE

RESEARCH ARTICLE

https://doi.org/10.1007/s10118-025-3275-0
Chinese J. Polym. Sci. **2025**, *43*, 429–438

Structural Difference in the Core-forming Block Reshapes RAFT-mediated Polymerization-induced Self-assembly

Yue-Xi Zhan[a], Li Zhang[a,b], Chun Feng[c*], and Jian-Bo Tan[a,b*]

[a] *Department of Polymeric Materials and Engineering, School of Materials and Energy, Guangdong University of Technology, Guangzhou 510006, China*
[b] *Guangdong Provincial Key Laboratory of Functional Soft Condensed Matter, Guangzhou 510006, China*
[c] *Shanghai Key Laboratory of Advanced Polymeric Materials, School of Materials Science and Engineering, East China University of Science and Technology, Shanghai 200237, China*

Electronic Supplementary Information

Abstract Polymerization-induced self-assembly (PISA) has become one of the most versatile approaches for scalable preparation of linear block copolymer nanoparticles with various morphologies. However, the controlled introduction of branching into the core-forming block and the effect on the morphologies of block copolymer nanoparticles under PISA conditions have rarely been explored. Herein, a series of multifunctional macromolecular chain transfer agents (macro-CTAs) were first synthesized by a two-step green light-activated photoiniferter polymerization using two types of chain transfer monomers (CTMs). These macro-CTAs were then used to mediate reversible addition-fragmentation chain transfer (RAFT) dispersion polymerization of styrene (St) to prepare block copolymers with different core-forming block structures and the assemblies. The effect of the core-forming block structure on the morphology of block copolymer nanoparticles was investigated in detail. Transmission electron microscopy (TEM) analysis indicated that the brush-like core-forming block structure facilitated the formation of higher-order morphologies, while the branched core-forming block structure favored the formation of lower-order morphologies. Moreover, it was found that using macro-CTAs with a shorter length also promoted the formation of higher-order morphologies. Finally, structures of block copolymers and the assemblies were further controlled by changing the structure of macro-CTA or using a binary mixture of two different macro-CTAs. We expect that this work not only sheds light on the synthesis of block copolymer nanoparticles but also provide important mechanistic insights into PISA of nonlinear block copolymers.

Keywords Polymerization-induced self-assembly; RAFT polymerization; Block copolymer nanoparticles; Branched structure

Citation: Zhan, Y. X.; Zhang, L.; Feng, C.; Tan, J. B. Structural difference in the core-forming block reshapes RAFT-mediated polymerization-induced self-assembly. *Chinese J. Polym. Sci.* **2025**, *43*, 429–438.

INTRODUCTION

Over the past ten years or so, polymerization-induced self-assembly (PISA) *via* reversible addition-fragmentation chain transfer (RAFT)-mediated dispersion polymerization has become a highly effective and versatile approach to prepare well-defined block copolymer nanoparticles.[1–30] Typically, RAFT-PISA involves growing a solvophobic block from a macromolecular RAFT (macro-RAFT) agent to form a block copolymer in a selective solvent. As the polymerization proceeds, *in situ* self-assembly occurs when the solvophobic block reaches to a critical molecular weight, leading to the formation of sterically-stabilized block copolymer nanoparticles. Compared with traditional solution self-assembly that usually performs at a diluted solution (<1 wt%),[31–34] such RAFT-PISA syntheses can be conducted at a highly concentrated solution with the solids being up to 50 wt%. Moreover, RAFT-PISA can eliminate the requirement for post-polymerization processing steps such as pH or solvent switch.

Currently, almost all RAFT-PISA formulations have been focused on the preparation of linear block copolymer nanoparticles using a monofunctional macro-RAFT agent. Morphologies of these block copolymer nanoparticles could be controlled by changing the solids content,[35,36] degrees of polymerization (DPs) of the solvophilic block and the solvophobic block,[37,38] reaction temperature,[36,39–41] polymerization kinetics,[42] and solvent composition,[19,43–45] *etc*. In contrast, the preparation of polymers with complex architectures by RAFT-PISA has rarely been explored. Indeed, it has been demonstrated that the polymer architecture had significant effects on the RAFT-PISA process as well as the morphology of polymer nanoparticles.[46–59] For example, An and co-workers[46] reported a direct comparison between AB_2 star block copolymers and AB diblock copolymers with comparable molecular

* Corresponding authors, E-mail: cfeng@ecust.edu.cn (C.F.)
E-mail: tanjianbo@gdut.edu.cn (J.B.T.)

Invited Research Article
Received October 28, 2024; Accepted November 21, 2024; Published online January 20, 2025

weights under aqueous RAFT-PISA conditions. They found that higher-order morphologies such as vesicles are favored in the case of AB_2 star block copolymers. Zhang and co-workers[47] also compared the performance of AB diblock copolymers and $(AB)_n$ star block copolymers in RAFT-PISA. They demonstrated that higher-order morphologies were favored in the case of $(AB)_n$ star block copolymers due to the enhanced fusion of polymer nanoparticles. Recently, our group[51] reported the preparation of segmented hyperbranched block copolymer nanoparticles by RAFT-PISA using segmented hyperbranched macro-RAFT agents with different RAFT group distributions. When using the R-type segmented hyperbranched macro-RAFT agent, flocculation occurred during the polymerization due to the bridging between polymer particles. When using the Z-type segmented hyperbranched macro-RAFT agent, the solvophobic block always grows in the inner of segmented hyperbranched block copolymers that can avoid bridging between polymer particles, and well-defined morphologies were obtained. Despite some achievements have been made on RAFT-PISA of nonlinear polymers, the effect of the core-forming block structure on RAFT-PISA has rarely been explored.

In this study, a series of multifunctional macro-RAFT agents were synthesized by a two-step green light-activated photoiniferter polymerization of two different RAFT chain transfer monomers (CTMs). These macro-RAFT agents were then employed to mediate RAFT dispersion polymerization of styrene (St), leading to the formation of block copolymers and the assemblies. These block copolymers share the same solvophilic block but with different solvophobic block structures. Effects of the core-forming block structure on RAFT-PISA as well as the morphology of polymer nanoparticles were investigated in detail.

EXPERIMENTAL

All experimental details are provided in the electronic supplementary information (ESI).

RESULTS AND DISCUSSION

Synthesis of Macro-RAFT Agents by Green Light-activated Photoiniferter Polymerization

For the synthesis of CTMs, 4-cyano-4-(ethylthiocarbonothioylthio)pentanoic acid (CEPA) and 2-(*n*-butyltrithiocarbonate)propionic acid (BTPA) were conjugated with hydroxyethyl methacrylate (HEMA) *via* esterification, denoted as CEPEMA and BTPEMA, respectively. According to the work reported by Shanmugam *et al.*,[60] the trithiocarbonate unit of CEPEMA can be activated under green light irradiation, while the trithiocarbonate unit of BTPEMA remains intact under green light irradiation. Fig. 1 shows ^{1}H-NMR spectra of CEPEMA and BTPEMA, confirming the successful formation of these compounds.

A two-step green light-activated photoiniferter polymerization was then performed to synthesize macro-RAFT agents (Scheme 1a). Specifically, a large batch of PPEGMA$_n$-CEPA was first synthesized by the green light-activated photoiniferter polymerization of PEGMA in 1,4-dioxane using CEPA. PPEGMA$_n$-CEPA was then chain-extended with CEPEMA or BTPEMA under green light-activated photoiniferter polymerization conditions. ^{1}H-NMR analysis confirmed near quantitative monomer conversions were achieved in both cases. Under green light irradiation, the polymerization of CEPEMA should undergo a self-condensing vinyl polymerization (SCVP) mechanism and linear-branched multifunctional macro-RAFT agents could be formed (Scheme 1a).[18] In contrast, the trithiocarbonate unit of BTPEMA did not involve in the photoiniferter polymerization and linear diblock copolymer multifunctional macro-RAFT agents should be formed (Scheme 1a). Fig. 2(a) shows size exclusion chromatography (SEC) traces of PPEGMA$_{15}$-CEPA, PPEGMA$_{15}$-PCEPEMA$_5$-CEPA, and PPEGMA$_{15}$-PBTPEMA$_5$-CEPA. It is apparent that the SEC trace shifted slightly to lower elution volume (higher molecular weight) after photoiniferter polymerization of CEPEMA or BTPEMA, suggesting the successful chain extension. Relatively narrow molecular weight distributions ($M_w/M_n \leq 1.20$) were observed for PPEGMA$_{15}$-CEPA and PPEGMA$_{15}$-PBTPEMA$_5$-CEPA. In con-

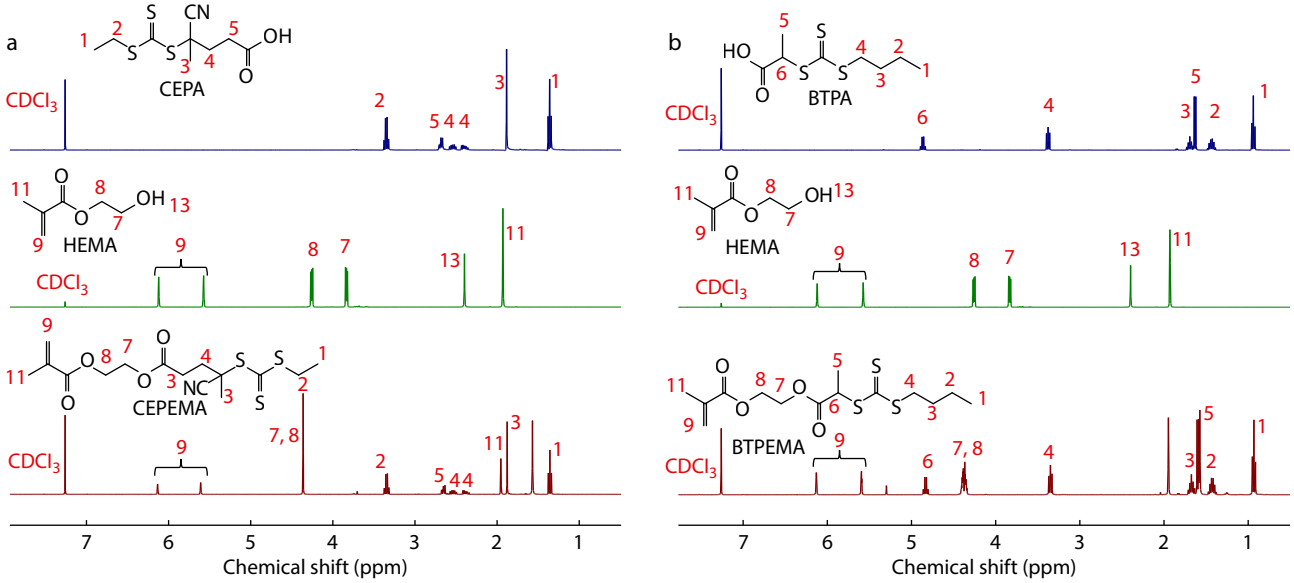

Fig. 1 (a) ^{1}H-NMR spectra of CEPA, HEMA and CEPEMA; (b) ^{1}H-NMR spectra of BTPA, HEMA and BTPEMA.

https://doi.org/10.1007/s10118-025-3275-0

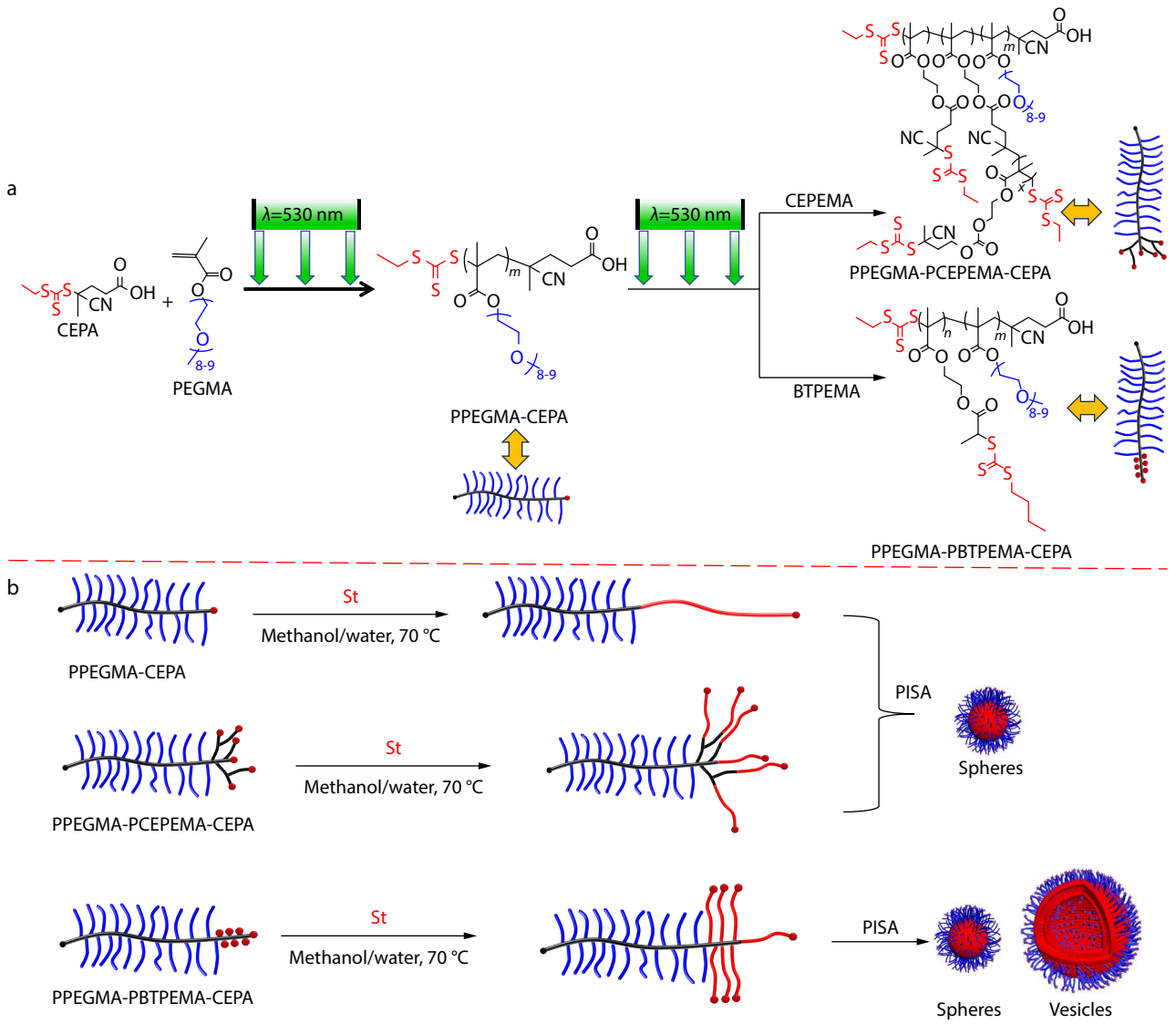

Scheme 1 (a) Schematic illustration for the synthesis of PPEGMA-CEPA, PPEGMA-PCEPEMA-CEPA, and PPEGMA-PBTPEMA-CEPA by green light-activated photoiniferter polymerization; (b) Schematic illustration for the RAFT-PISA process using PPEGMA-CEPA, PPEGMA-PCEPEMA-CEPA, or PPEGMA-PBTPEMA-CEPA as the macro-RAFT agent.

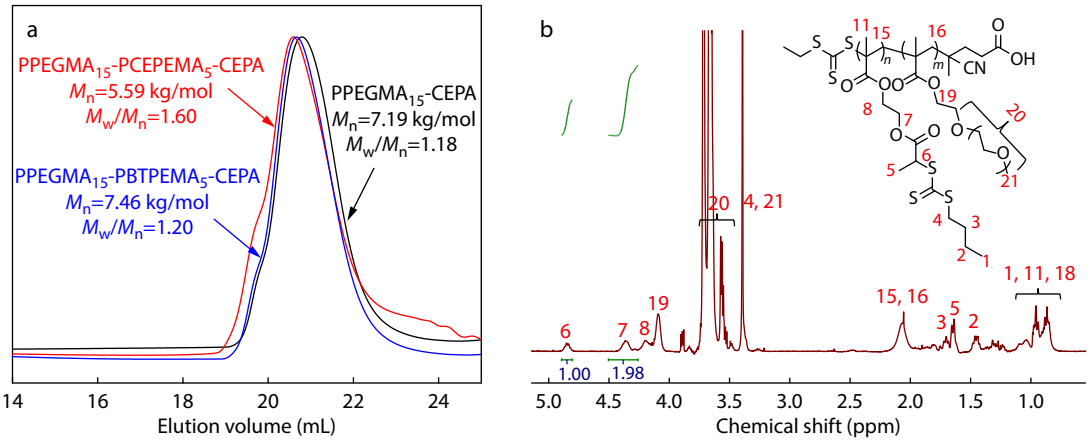

Fig. 2 (a) THF SEC traces of $PPEGMA_{15}$-CEPA, $PPEGMA_{15}$-$PCEPEMA_5$-CEPA, and $PPEGMA_{15}$-$PBTPEMA_5$-CEPA; (b) ^{1}H-NMR spectrum of $PPEGMA_{15}$-$PBTPEMA_5$-CEPA.

https://doi.org/10.1007/s10118-025-3275-0

trast, a relatively broad molecular weight distribution was observed (M_w/M_n=1.60) for PPEGMA$_{15}$-PCEPEMA$_5$-CEPA due to the formation of branched structure *via* SCVP. Fig. 2(b) shows the ^{1}H-NMR spectrum of PPEGMA$_{15}$-PBTPEMA$_5$-CEPA in $CDCl_3$. The presence of a proton signal at ~4.75 ppm indicates that the trithiocarbonate group of BTPEMA was retained after polymerization. The integra of peak 7 (~4.35 ppm) is almost twice that of peak 6 (~4.75 ppm), suggesting that the trithiocarbonate group of the BTPEMA unit did not involve in the photoiniferter polymerization.

RAFT Dispersion Polymerization of Styrene Using Multifunctional Macro-RAFT Agents

As a control experiment, PPEGMA$_{15}$-CEPA was first employed to mediate RAFT dispersion polymerization of St (20 wt%) in methanol/water (80/20, *W*/*W*) with different [St]/[PPEGMA$_{15}$-CEPA] ratios. The choice of St as the monomer is due to the good controllability of trithiocarbonate group of BTPEMA and CEPA toward St and the relatively high glass transition temperature of PSt. In this case, diblock copolymers of PPEGMA$_{15}$-PSt$_n$ with a linear core-forming block would be formed (Scheme 1b). Fig. S1 (in ESI) shows SEC traces of the formed diblock copolymers. Relatively narrow molecular weight distributions ($M_w/M_n \leq$ 1.41) were observed in all cases, suggesting the formation of well-defined block copolymers. The presence of a high-molecular-weight shoulder in each case should be attributed to the occurrence of bimolecular termination during RAFT dispersion polymerization. Figs. 3(a)–3(d) show transmission electron microscopy (TEM) images of the formed block copolymer nanoparticles. At all investigated [St]/[PPEGMA$_{15}$-CEPA] ratios, pure spheres were observed. Hydrodynamic diameters of these spheres were also determined by dynamic light scattering (DLS) and it was found that the hydrodynamic diameter increased with the [St]/[PPEGMA$_{15}$-CEPA] (Fig. 3e). The formation of kinetically-trapped spheres in this case should be attributed to the weak mobility of PSt core-forming block under these conditions,[1] which is not beneficial for the re-organization of polymer chains. Branched or brush-like polymers with relatively short side chains that can avoid chain-chain interchain entanglement.[61] Therefore, the introduction of branching in the core-forming block is an attractive strategy to improve the mobility of the core-forming block.[52] Moreover, the effective stabilization of PPEGMA$_{15}$ toward micelles can inhibit the fusion between micelles, which can be improved by using macro-RAFT agents with a shorter length.[35,37]

In order to introduce branching in the core-forming block, two multifunctional macro-RAFT agents, PPEGMA$_{15}$-PCEPEMA$_5$-CEPA and PPEGMA$_{15}$-PBTPEMA$_5$-CEPA, were then used to mediate RAFT dispersion polymerization of St (20 wt%) in methanol/water (80/20, *W*/*W*) with different [St]/[macro-RAFT] ratios. It should be noted that both CEPA and BTPA exhibit good controllability toward St.[62] In all cases, high monomer conversions were achieved within 24 h of polymerization, as verified by ^{1}H-NMR spectroscopy. When using PPEGMA$_{15}$-PCEPEMA$_5$-CEPA, linear-branched block copolymers should be formed (Scheme 1b). As shown in Figs. 4(a)–4(d), spherical micelles were formed at all investigated [St]/[macro-RAFT] ratios. In contrast, brush-like block copolymers should be formed when using PPEGMA$_{15}$-PBTPEMA$_5$-CEPA as the macro-RAFT agent (Scheme 1b). At [St]/[macro-RAFT] ratios of 200 and 250, mixed morphologies of vesicles and spheres were observed (Figs. 4e and 4f). When the [St]/[macro-RAFT] ratio was increased to 300, pure vesicles were formed (Fig. 4g). Further increasing the [St]/[macro-RAFT] ratio to 350 led to the formation of porous vesicles (Fig. 4h). The obtained polymers were also analyzed by SEC and multimodal SEC traces was observed in each case (Fig. S2 in ESI). This can be explained by the fact that both PPEGMA$_{15}$-PCEPEMA$_5$-CEPA and PPEGMA$_{15}$-PBTPEMA$_5$-CEPA should be mixtures of polymers with different number of trithiocarbonate groups, although the average number of CEPEMA or BTPEMA was 5. It should be noted that the presence of a low-molecular-weight peak in each case should be attributed to the presence of a small amount of PCEPEMA and PBTPEMA in the macro-RAFT agents.[60,62,63] To further illustrate the morphological difference between these two formulations, two morphological phase diagrams were constructed by changing the monomer concentration and the [St]/[macro-RAFT] ratio. As shown in Fig. 5(a), only spheres were obtained in the case of PPEGMA$_{15}$-PCEPEMA$_5$-CEPA even at a 25 wt% St concentration with the [St]/[macro-RAFT] ratio being up to 350. In

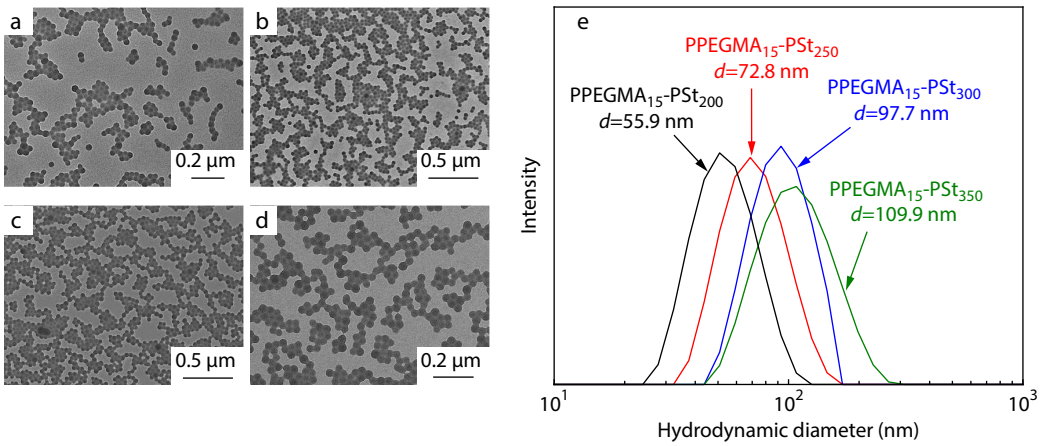

Fig. 3 (a–d) TEM images of block copolymer nanoparticles prepared by RAFT dispersion polymerization of St (20 wt%) using PPEGMA$_{15}$-CEPA with different [St]/[PPEGMA$_{15}$-CEPA] ratios: (a) 200, (b) 250, (c) 300, (d) 350; (e) DLS distributions of PPEGMA$_{15}$-PSt$_n$ (*n*=200, 250, 300, 350) block copolymer nanoparticles prepared by RAFT dispersion polymerization of St (20 wt%) using PPEGMA$_{15}$-CEPA.

https://doi.org/10.1007/s10118-025-3275-0

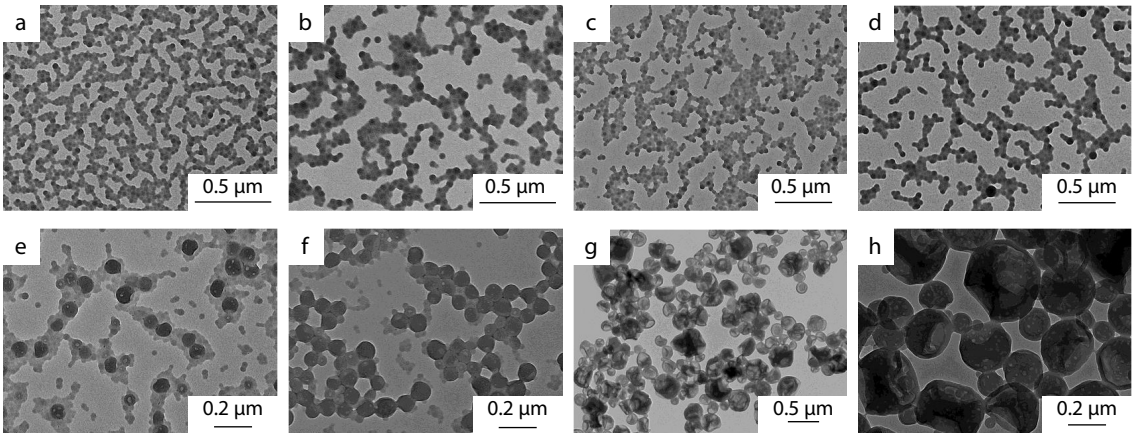

Fig. 4 TEM images of block copolymer nanoparticles prepared by RAFT dispersion polymerization of St (20 wt%) using (a–d) PPEGMA$_{15}$-PCEPEMA$_5$-CEPA or (e–h) PPEGMA$_{15}$-PBTPEMA$_5$-CEPA with different [St]/[macro-RAFT] ratios: (a, e) 200, (b, f) 250, (c, g) 300, (d, h) 350.

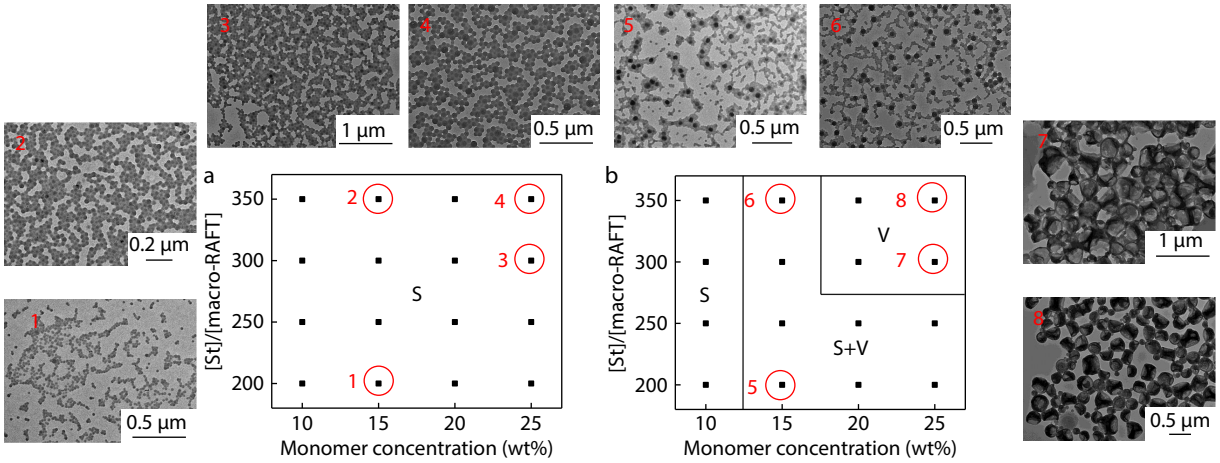

Fig. 5 Morphological phase diagrams for block copolymer nanoparticles prepared by RAFT dispersion polymerization of St (20 wt%) using either (a) PPEGMA$_{15}$-PCEPEMA$_5$-CEPA or (b) PPEGMA$_{15}$-PBTPEMA$_5$-CEPA by varying monomer concentrations and [St]/[macro-RAFT] ratios. Phase regions consist of spheres (S) and vesicles (V).

contrast, a large region of mixed morphologies consist of spheres and vesicles was observed in the case of PPEGMA$_{15}$-PBTPEMA$_5$-CEPA (Fig. 5b). This morphological phase diagram is concentration-dependent with pure vesicles only being formed at the St concentration of 20 wt% or higher. These results suggest that the brush-like structure of core-forming block facilitates the formation of higher-order morphologies as compared to the branched structure of core-forming block under PISA conditions. This may be explained by the fact that the regularity of PSt side chains in the case of PPEGMA$_n$-PBTPEMA$_5$-CEPA is better than that in the case of PPEGMA$_n$-PCEPEMA$_5$-CEPA, which is important for the efficient packing of block copolymers and therefore the morphological evolution. Moreover, molecular weight distributions of block copolymers synthesized by using PPEGMA$_{15}$-PBTPEMA$_5$-CEPA are narrower than those synthesized by using PPEGMA$_{15}$-PCEPEMA$_5$-CEPA (Fig. 2a), which should also affect the self-assembly process.[64] It should be noted that no worm-like morphology was observed in these two phase diagrams. Indeed, for PISA formulations of polystyrene-based block copolymers, it is always difficult to achieve worm-like morphology by varying reaction parameters.[20,65]

Another useful approach to promote the morphological evolution during PISA is the utilization of macro-RAFT agents with lower molecular weights.[35,37] PPEGMA$_{10}$-CEPA, PPEGMA$_{10}$-PCEPEMA$_5$-CEPA and PPEGMA$_{10}$-PBTPEMA$_5$-CEPA were also synthesized by green light-activated photoiniferter polymerization of CEPEMA or BTPEMA using PPEGMA$_{10}$-CEPA as the first block (Fig. S3 in ESI). These three macro-RAFT agents were then used to mediate RAFT dispersion polymerization of St with different [St]/[macro-RAFT] ratios. In the case of PPEGMA$_{10}$-PBTPEMA$_5$-CEPA, vesicles with porous internal structures were formed at all investigated [St]/[macro-RAFT] ratios (Figs. 6a–6d). By using PPEGMA$_{10}$-PCEPEMA$_5$-CEPA as the macro-RAFT agent, spheres were formed at [St]/[macro-RAFT] ratios of 300 or lower (Fig. 6e–6g). Further increasing the [St]/[macro-RAFT] ratio to 350 led to the formation of spheres mixed with porous vesicles (Fig. 6h). By using PPEGMA$_{10}$-CEPA as the macro-RAFT agent, only spheres were formed at all investigated [St]/[macro-RAFT] ratios (Figs. 6i–6l). These results are consistent with RAFT dispersion polymerization of St mediated by PPEGMA$_{15}$-CEPA, PPEGMA$_{15}$-PCEPEMA$_5$-CEPA, and PPEGMA$_{15}$-PBTPEMA$_5$-CEPA. Comparing Fig. 4 and Fig. 6, it is apparent that decreasing the molec-

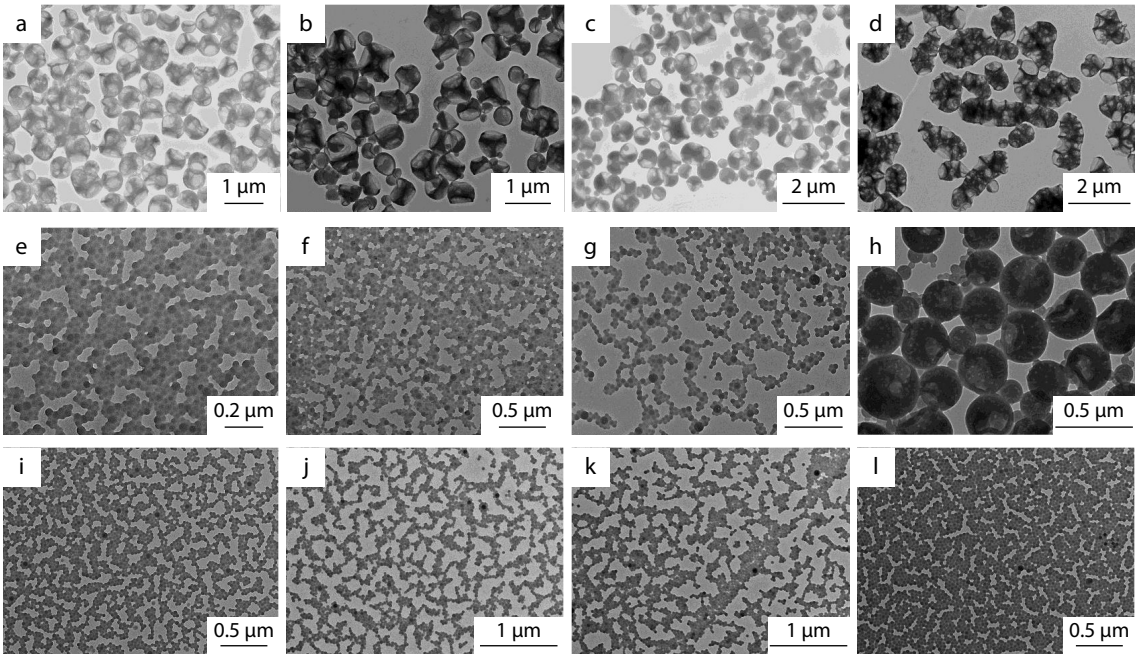

Fig. 6 TEM images of block copolymer nanoparticles prepared by RAFT dispersion polymerization of St (20 wt%) using (a–d) $PPEGMA_{10}$-$PBTPEMA_5$-CEPA or (e–h) $PPEGMA_{10}$-$PCEPEMA_5$-CEPA or (i–l) $PPEGMA_{10}$-CEPA with different [St]/[macro-RAFT] ratios: (a, e, i) 200, (b, f, j) 250, (c, g, k) 300, (d, h, l) 350.

ular weight of the stabilizer block could promote the formation of higher-order morphologies. This is because the shorter length of the stabilizer block should provide poorer stabilization toward particles that should facilitate the collision and fusion between particles, which is important for the morphological evolution to higher-order morphologies.

To further investigate the polymerization process, kinetic studies of RAFT dispersion polymerization of St (20 wt%) using $PPEGMA_{15}$-$PCEPEMA_5$-CEPA and $PPEGMA_{15}$-$PBTPEMA_5$-CEPA were then performed ([St]/[macro-RAFT]=300). In both cases, near quantitative monomer conversions (>99%) were achieved within 12 h of polymerization (Fig. 7a). For the polymerization using $PPEGMA_{15}$-$PCEPEMA_5$-CEPA, the corresponding semilogarithmic plot indicate a dramatic increase in the polymerization rate after ~5.1 h (blue plot in Fig. 7b), which corresponds to a St conversion of 41.6%. Such observation is typical in previously reported PISA formulations,[66–68] which corresponds to the onset of micellar nucleation. Similar results are observed in the case of $PPEGMA_{15}$-$PBTPEMA_5$-CEPA (red plot in Fig. 7b). It was found that the nucleation stage for the polymerization using $PPEGMA_{15}$-$PBTPEMA_5$-CEPA was shorter than that of using $PPEGMA_{15}$-$PCEPEMA_5$-CEPA. This should be attributed to the structural difference in the core-forming block and the difference in the molecular weight distribution. Each sample withdrawn for these kinetic studies was also characterized by SEC. Multimodal SEC traces were observed for all samples (Figs. 7c and 7e). This is because the samples should be mixtures of polymers with different number of PSt side chains. It should be noted that a low-molecular-weight shoulder was observed in each case, which can be attributed to the presence of a small amount of PBTPEMA or PCEPEMA in the macro-RAFT agents. Figs. 7(d) and 7(f) show the evolution of number-average molecular weight (M_n) and M_w/M_n with monomer conversion during RAFT dispersion polymerization of St. In the case $PPEGMA_{15}$-$PBTPEMA_5$-CEPA, a linear evolution of M_n with monomer conversion was observed (Fig. 7f), suggesting the polymerization is well-controlled. It should be noted that relatively high M_w/M_n values were observed throughout the polymerization. However, the M_n value did not increase linearly with monomer conversion when using $PPEGMA_{15}$-$PCEPEMA_5$-CEPA (Fig. 7d), which can be attributed to the branched structure of the block copolymer.

Further Structural Control Over Block Copolymers and Morphological Control Over Polymer Assemblies

The above results demonstrate that the core-forming block structure has significant influence on the formed polymer assemblies. Taking advantage of the different reactivity of BTPEMA and CEPEMA under green light irradiation, the structure of macro-RAFT agents can be further controlled by using a binary mixture of CEPEMA and BTPEMA with different [CEPEMA]/[BTPEMA] ratios. $PPEGMA_{15}$-P($CEPEMA_{3.5}$-*co*-$BTPEMA_{1.5}$)-CEPA and $PPEGMA_{15}$-P($CEPEMA_{1.5}$-*co*-$BTPEMA_{3.5}$)-CEPA were also synthesized by green light-activated photoiniferter polymerization using $PPEGMA_{15}$-CEPA (Fig. S4 in ESI). These two macro-RAFT agents were then employed to mediate RAFT dispersion polymerization of St (20 wt%) with different [St]/[macro-RAFT] agent. Figs. 8(a)–8(h) show TEM images of the obtained polymer assemblies, and mixed morphologies of spheres and porous vesicles were observed in all cases. Combining the data of Fig. 4 and Fig. 8(a)–8(h), a morphological phase diagram for RAFT dispersion polymerization of St mediated by $PPEGMA_{15}$-P($CEPEMA_n$-*co*-$BTPEMA_m$)-CEPA ($m + n = 5$) was then constructed by varying the [St]/[macro-RAFT] ratio and the [CEPEMA]/[BTPEMA] ratio. As shown in Fig. 8(i), it is apparent that decreasing the [CEPEMA]/[BTPEMA] ratio would facilitate the formation of poly-

https://doi.org/10.1007/s10118-025-3275-0

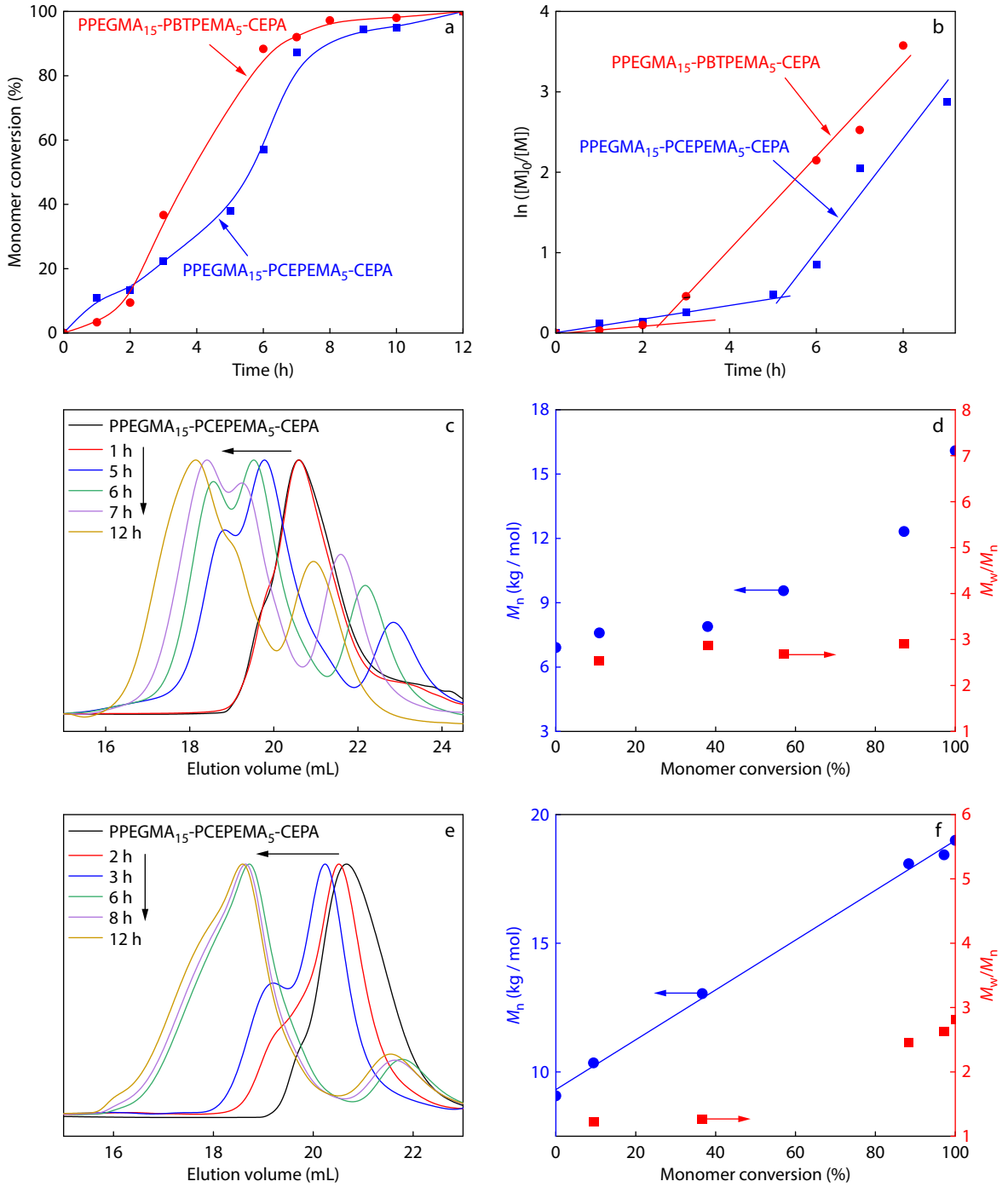

Fig. 7 (a) Polymerization kinetics for RAFT dispersion polymerization of St (20 wt%) mediated by PPEGMA$_{15}$-PBTPEMA$_5$-CEPA (red plot) or PPEGMA$_{15}$-PCEPEMA$_5$-CEPA (blue plot) with the [St]/[macro-RAFT] ratio of 300/1; (b) Semilogarithmic plots of RAFT dispersion polymerization of St (20 wt%) mediated by PPEGMA$_{15}$-PBTPEMA$_5$-CEPA (red plot) or PPEGMA$_{15}$-PCEPEMA$_5$-CEPA (blue plot) with the [St]/[macro-RAFT] ratio of 300/1; (c, e) THF SEC traces and (d, f) evolution of M_n and M_w/M_n with monomer conversion for polymers obtained during RAFT dispersion polymerization of St (20 wt%) mediated by (c, d) PPEGMA$_{15}$-PCEPEMA$_5$-CEPA or (e, f) PPEGMA$_{15}$-PBTPEMA$_5$-CEPA with the [St]/[macro-RAFT] ratio of 300/1.

mer assemblies with high-order morphologies. Pure vesicles could only be obtained when using PPEGMA$_{15}$-PBTPEMA$_5$-CEPA, while pure spheres were obtained when using PPEGMA$_{15}$-PCEPEMA$_5$-CEPA. These results further confirm that the brush-like core-forming block is more likely to form higher-order morphologies than the branched core-forming block. In other words, the core-forming block structure could be served as an effective parameter to tune morphologies of polymer assemblies under PISA conditions.

To further control the morphology of polymer assemblies, we also performed RAFT dispersion polymerization of St (20 wt%) using a binary mixture of PPEGMA$_{10}$-PBTPEMA$_5$-CEPA

https://doi.org/10.1007/s10118-025-3275-0

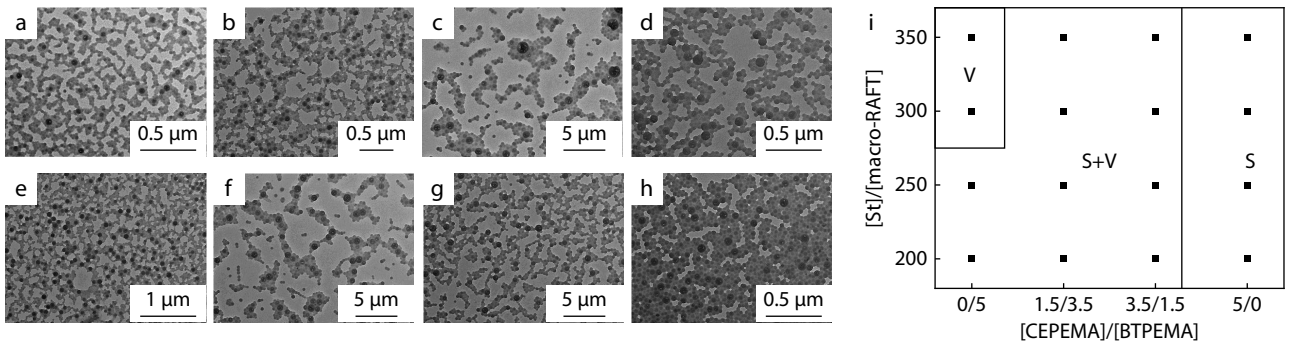

Fig. 8 (a–h) TEM images of block copolymer nanoparticles prepared by RAFT dispersion polymerization of St (20 wt%) using (a–d) $PPEGMA_{15}$-$P(CEPEMA_{3.5}$-*co*-$BTPEMA_{1.5})$-CEPA or (e–h) $PPEGMA_{15}$-$P(CEPEMA_{1.5}$-*co*-$BTPEMA_{3.5})$-CEPA with different [St]/[macro-RAFT] ratios: (a, e) 200, (b, f) 250, (c, g) 300, (d, h) 350; (i) Morphological phase diagram for block copolymer nanoparticles prepared by RAFT dispersion polymerization of St (20 wt%) using $PPEGMA_{15}$-$P(CEPEMA_n$-*co*-$BTPEMA_m)$-CEPA by varying the [CEPEMA]/[BTPEMA] ratio and the [St]/[macro-RAFT] ratio. Phase regions consist of spheres (S) and vesicles (V).

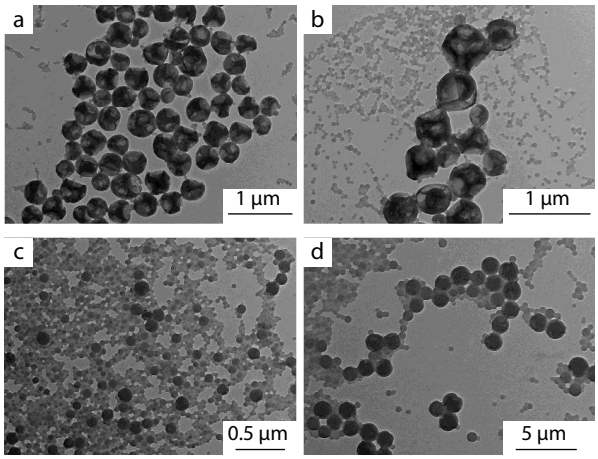

Fig. 9 TEM images of block copolymer nanoparticles prepared by RAFT dispersion polymerization of St (20 wt%) using a binary mixture of $PPEGMA_{10}$-$PBTPEMA_5$-CEPA and $PPEGMA_{10}$-$PCEPEMA_5$-CEPA with different [$PPEGMA_{10}$-$PBTPEMA_5$-CEPA]/[$PPEGMA_{10}$-$PCEPEMA_5$-CEPA] ratios: (a) 8/2, (b) 6/4, (c) 4/6, (d) 2/8.

and $PPEGMA_{10}$-$PCEPEMA_5$-CEPA with different [$PPEGMA_{10}$-$PBTPEMA_5$-CEPA]/[$PPEGMA_{10}$-$PCEPEMA_5$-CEPA] ratios (8/2, 6/4, 4/6, and 2/8). Fig. 9 shows TEM images of the formed polymer assemblies. It should be noted that the TEM images of polymer assemblies prepared at the [$PPEGMA_{10}$-$PBTPEMA_5$-CEPA]/[$PPEGMA_{10}$-$PCEPEMA_5$-CEPA] ratio of 10/0 and 0/10 are shown in Fig. 6(c) and Fig. 6(g), respectively. As decreasing the [$PPEGMA_{10}$-$PBTPEMA_5$-CEPA]/[$PPEGMA_{10}$-$PCEPEMA_5$-CEPA] ratio, it is apparent that the morphology transformed from pure vesicles to mixed morphologies of vesicles and spheres to spheres. These results further confirmed that the brush-like core-forming block structure favored the formation of higher-order morphologies than the branched core-forming block structure.

CONCLUSIONS

In summary, multifunctional macro-RAFT agents were successfully synthesized by photoiniferter polymerization of CEPEMA or BTPEMA using $PPEGMA_n$-CEPA as the first block. These macro-RAFT agents were then employed to mediate RAFT dispersion polymerization of St to prepare block copolymers with branched core-forming block or brush-like core-forming block. TEM analysis indicated that the branched core-forming favored the formation of lower-order morphologies such as spheres while the brush-like core-forming block facilitated the formation of higher-order morphologies such as vesicles. It was found that using a shorter solvophilic block ($PPEGMA_n$) also facilitated the formation of higher-order morphologies. Kinetic studies indicated that high monomer conversions (>99%) were achieved within 12 h of polymerization. SEC analysis of the formed block copolymers indicated that multimodal SEC traces and broad molecular weight distributions were observed in all cases. Finally, the morphology of block copolymer assemblies could be further controlled by using $PPEGMA_{15}$-$P(CEPEMA_n$-*co*-$BTPEMA_m)$-CEPA with different [CEPEMA]/[BTPEMA] ratios or using a binary mixture of $PPEGMA_{10}$-$PBTPEMA_5$-CEPA and $PPEGMA_{10}$-$PCEPEMA_5$-CEPA with different [$PPEGMA_{10}$-$PBTPEMA_5$-CEPA]/[$PPEGMA_{10}$-$PCEPEMA_5$-CEPA] ratios.

Conflict of Interests

The authors declare no interest conflict.

Electronic Supplementary Information

Electronic supplementary information (ESI) is available free of charge in the online version of this article at http://doi.org/10.1007/s10118-025-3275-0.

Data Availability Statement

The related data of this paper is data that should not be shared, and can be obtained from the author for reasonable reasons. The author's contact information: tanjianbo@gdut.edu.cn.

ACKNOWLEDGMENTS

This work was financially supported by the National Natural Science Foundation of China (Nos. 22171055 and 52222301), the Guangdong Natural Science Foundation for Distinguished

Young Scholar (No. 2022B1515020078), and the Science and Technology Program of Guangzhou (No. 2024A04J2821). They would like to thank Wei Song of Analysis and Test Center of Guangdong University of technology for DLS measurement.

REFERENCES

1 Wan, W. M.; Hong, C. Y.; Pan, C. Y. One-pot synthesis of nanomaterials *via* RAFT polymerization induced self-assembly and morphology transition. *Chem. Commun.* **2009**, *39*, 5883–5885.
2 Liu, C.; Hong, C. Y.; Pan, C. Y. Polymerization techniques in polymerization-induced self-assembly (PISA). *Polym. Chem.* **2020**, *11*, 3673–3689.
3 Zhang, W. J.; Hong, C. Y.; Pan, C. Y. Polymerization-induced self-assembly of functionalized block copolymer nanoparticles and their application in drug delivery. *Macromol. Rapid Commun.* **2019**, *40*, 1800279.
4 Zhu, R. M.; Chang, Z. X.; Zhang, W. J.; Hong, C. Y. Polymerization-induced self-assembly with assistance of aromatic interactions facilitates the formation of polymeric nanotubes. *Macromolecules* **2023**, *56*, 3296–3303.
5 Kadirkhanov, J.; Yang, C. L.; Chang, Z. X.; Zhu, R. M.; Pan, C. Y.; You, Y. Z.; Zhang, W. J.; Hong, C. Y. *In situ* cross-linking polymerization-induced self-assembly not only generates cross-linked structures but also promotes morphology transition by the cross-linker. *Polym. Chem*. **2021**, *12*, 1768–1775.
6 An, Z.; Shi, Q.; Tang, W.; Tsung, C. K.; Hawker, C. J.; Stucky, G. D. Facile RAFT precipitation polymerization for the microwave-assisted synthesis of well-defined, double hydrophilic block copolymers and nanostructured hydrogels. *J. Am. Chem. Soc.* **2007**, *129*, 14493–14499.
7 Lv, F.; An, Z.; Wu, P. Efficient access to inverse bicontinuous mesophases *via* polymerization-induced cooperative assembly. *CCS Chem.* **2020**, *3*, 2211–2222.
8 Zhu, A.; Lv, X.; Shen, L.; Zhang, B.; An, Z. Polymerization-induced cooperative assembly of block copolymer and homopolymer *via* RAFT dispersion polymerization. *ACS Macro Lett.* **2017**, *6*, 304–309.
9 Wang, X.; Shen, L.; An, Z. Dispersion polymerization in environmentally benign solvents *via* reversible deactivation radical polymerization. *Prog. Polym. Sci.* **2018**, *83*, 1–27.
10 Li, S.; Han, G.; Zhang, W. Cross-linking approaches for block copolymer nano-assemblies *via* RAFT-mediated polymerization-induced self-assembly. *Polym. Chem.* **2020**, *11*, 4681–4692.
11 Pang, B.; Liu, Y.; Cao, R.; Zhang, W. Hybrid nanoscale vesicles of polyhedral oligomeric silsesquioxane-based star block copolymers for thermal insulation applications. *ACS Appl. Nano Mater.* **2022**, *5*, 7042–7050.
12 Huang, J.; Guo, Y.; Gu, S.; Han, G.; Duan, W.; Gao, C.; Zhang, W. Multicompartment block copolymer nanoparticles: recent advances and future perspectives. *Polym. Chem.* **2019**, *10*, 3426–3435.
13 Wang, L.; Ding, Y.; Liu, Q.; Zhao, Q.; Dai, X.; Lu, X.; Cai, Y. Sequence-controlled polymerization-induced self-assembly. *ACS Macro Lett.* **2019**, *8*, 623–628.
14 Cao, L.; Zhao, Q.; Liu, Q.; Ma, L.; Li, C.; Wang, X.; Cai, Y. Electrostatic manipulation of triblock terpolymer nanofilm compartmentalization during aqueous photoinitiated polymerization-induced self-assembly. *Macromolecules* **2020**, *53*, 2220–2227.
15 Wang, Y.; Li, C.; Ma, L.; Wang, X.; Wang, K.; Lu, X.; Cai, Y. Interfacial liquid-liquid phase separation-driven polymerization-induced electrostatic self-assembly. *Macromolecules* **2021**, *54*, 5577–5585.
16 Ding, Y.; Cai, M.; Cui, Z.; Huang, L.; Wang, L.; Lu, X.; Cai, Y. Synthesis of low-dimensional polyion complex nanomaterials *via* polymerization-induced electrostatic self-assembly. *Angew. Chem. Int. Ed.* **2018**, *57*, 1053–1056.
17 Guan, S.; Chen, A. Influence of spacer lengths on the morphology of biphenyl-containing liquid crystalline block copolymer nanoparticles *via* polymerization-induced self-assembly. *Macromolecules* **2020**, *53*, 6235–6245.
18 Li, Y.; Li, Y.; Yan, R.; Zhang, L.; Liu, H.; Tan, J. Chain architecture as an orthogonal parameter to tune morphologies of polymer assemblies: efficient synthesis and self-assembly of linear-branched block copolymers *via* RAFT dispersion polymerization. *Macromolecules* **2024**, *57*, 5175–5188.
19 Cao, J.; Li, Y.; Tan, Y.; Zhang, L.; Tan, J. From RAFT emulsion polymerization to RAFT dispersion polymerization: a facile approach to tuning dispersities and behaviors of self-assembled block copolymers. *Polym. Chem.* **2024**, *15*, 106–117.
20 Li, Z.; Wang, R.; Luo, X.; Zhang, L.; Tan, J. ABC or ACB triblock copolymers? Changing the RAFT group position in diblock copolymer macro-RAFT agents leads to different PISA behaviors in RAFT dispersion polymerization. *Polym. Chem.* **2024**, *15*, 1736–1747.
21 Niu, B.; Huang, H.; Zhang, L.; Tan, J. Grafting block copolymer nanoparticles to a surface *via* aqueous photoinduced polymerization-induced self-assembly at room temperature. *ACS Macro Lett.* **2024**, *13*, 577–585.
22 He, J.; Chen, Y.; Zhang, L.; Tan, J. Oxidation-responsive framboidal triblock copolymer vesicles prepared by photoinitiated RAFT seeded emulsion polymerization. *Chin. Chem. Lett.* **2023**, *34*, 107344.
23 Zhao, S.; Zhang, L.; Tan, J. *In situ* synthesis of branched block copolymer assemblies *via* raft dispersion polymerization using branched macro-RAFT agents. *Chin. J. Chem*. **2023**, *41*, 1517–1525.
24 Zhou, J.; Huang, Q.; Zhang, L.; Tan, J. Exploiting the monomer-feeding mechanism of RAFT emulsion polymerization for polymerization-induced self-assembly of asymmetric divinyl monomers. *ACS Macro Lett.* **2023**, *12*, 1457–1465.
25 Canning, S. L.; Smith, G. N.; Armes, S. P. A critical appraisal of RAFT-mediated polymerization-induced self-assembly. *Macromolecules* **2016**, *49*, 1985–2001.
26 Penfold, N. J. W.; Yeow, J.; Boyer, C.; Armes, S. P. Emerging trends in polymerization-induced self-assembly. *ACS Macro Lett.* **2019**, *8* (8), 1029–1054.
27 Warren, N. J.; Armes, S. P. Polymerization-induced self-assembly of block copolymer nano-objects *via* RAFT aqueous dispersion polymerization. *J. Am. Chem. Soc.* **2014**, *136*, 10174–10185.
28 Yeow, J.; Boyer, C. Photoinitiated polymerization-induced self-assembly (photo-PISA): new insights and opportunities. *Adv. Sci.* **2017**, *4*, 1700137.
29 Lin, D.; Zhang, L.; Tan, J. Room-temperature heterogeneous reversible deactivation radical polymerization. *Acta Polymerica Sinica* (in Chinese) **2023**, *54*, 761–777.
30 Xiang, J. Y.; Zhang, W. L.; Li, H. T.; He, Y. N. pH induced self-assembly of AIE fluorescent probe for tumor imaging. *Chinese J. Polym. Sci*. **2024**, *42*, 7–13.
31 Du, J.; Tang, Y.; Lewis, A. L.; Armes, S. P. pH-sensitive vesicles based on a biocompatible zwitterionic diblock copolymer. *J. Am. Chem. Soc*. **2005**, *127*, 17982–17983.
32 Du, J.; Sun, H. Polymer/TiO_2 hybrid vesicles for excellent uv screening and effective encapsulation of antioxidant agents. *ACS Appl. Mater. Interfaces* **2014**, *6*, 13535–13541.
33 Gao, Y.; Qiu, H.; Zhou, H.; Li, X.; Harniman, R.; Winnik, M. A.; Manners, I. Crystallization-driven solution self-assembly of block copolymers with a photocleavable junction. *J. Am. Chem. Soc.* **2015**, *137*, 2203–2206.
34 Song, Y.; Xiang, B.; Huang, X. Y.; Lu, G.-L.; Feng, C. Living crystallization-driven self-assembly of oligo(p-phenylene vinylene)-containing block copolymers: impact of branched structure of alkyl side chain of π-conjugated segment. *Chinese J. Polym. Sci.* **2023**, *41*, 574–584.

https://doi.org/10.1007/s10118-025-3275-0

35 Blanazs, A.; Ryan, A. J.; Armes, S. P. Predictive phase diagrams for RAFT aqueous dispersion polymerization: effect of block copolymer composition, molecular weight, and copolymer concentration. *Macromolecules* **2012**, *45*, 5099–5107.
36 Tan, J.; Liu, D.; Bai, Y.; Huang, C.; Li, X.; He, J.; Xu, Q.; Zhang, X.; Zhang, L. An insight into aqueous photoinitiated polymerization-induced self-assembly (photo-PISA) for the preparation of diblock copolymer nano-objects. *Polym. Chem.* **2017**, *8*, 1315–1327.
37 Tan, J.; Bai, Y.; Zhang, X.; Zhang, L. Room temperature synthesis of poly(poly(ethylene glycol) methyl ether methacrylate)-based diblock copolymer nano-objects via photoinitiated polymerization-induced self-assembly (photo-PISA). *Polym. Chem.* **2016**, *7*, 2372–2380.
38 Jones, E. R.; Semsarilar, M.; Blanazs, A.; Armes, S. P. Efficient synthesis of amine-functional diblock copolymer nanoparticles *via* RAFT dispersion polymerization of benzyl methacrylate in alcoholic media. *Macromolecules* **2012**, *45*, 5091–5098.
39 He, J.; Liu, D.; Tan, J.; Zhang, L. Sodium bis(acyl)phosphane oxide (SBAPO): an efficient photoinitiator for blue light initiated aqueous RAFT dispersion Polymerization. *Polymer* **2018**, *145*, 70–79.
40 Ma, Y.; Gao, P.; Ding, Y.; Huang, L.; Wang, L.; Lu, X.; Cai, Y. Visible light initiated thermoresponsive aqueous dispersion polymerization-induced self-assembly. *Macromolecules* **2019**, *52*, 1033–1041.
41 Blackman, L. D.; Doncom, K. E. B.; Gibson, M. I.; O'Reilly, R. K. Comparison of photo- and Thermally Initiated Polymerization-induced self-assembly: a lack of end group fidelity drives the formation of higher order morphologies. *Polym. Chem.* **2017**, *8*, 2860–2871.
42 Luo, X.; Zhao, S.; Chen, Y.; Zhang, L.; Tan, J. Switching between thermal initiation and photoinitiation redirects RAFT-mediated polymerization-induced self-assembly. *Macromolecules* **2021**, *54*, 2948–2959.
43 Gao, C.; Zhou, H.; Qu, Y.; Wang, W.; Khan, H.; Zhang, W. *In Situ* synthesis of block copolymer nanoassemblies *via* polymerization-induced self-assembly in poly(ethylene glycol). *Macromolecules* **2016**, *49*, 3789–3798.
44 Lv, F.; An, Z.; Wu, P. What determines the formation of block copolymer nanotubes. *Macromolecules* **2020**, *53*, 367–373.
45 Jones, E. R.; Semsarilar, M.; Wyman, P.; Boerakker, M.; Armes, S. P. Addition of water to an Alcoholic RAFT PISA formulation leads to faster kinetics but limits the evolution of copolymer morphology. *Polym. Chem.* **2016**, *7*, 851–859.
46 Wang, X.; Figg, C. A.; Lv, X.; Yang, Y.; Sumerlin, B. S.; An, Z. Star architecture promoting morphological transitions during polymerization-induced self-assembly. *ACS Macro Lett.* **2017**, *6*, 337–342.
47 Zhang, Y.; Cao, M.; Han, G.; Guo, T.; Ying, T.; Zhang, W. Topology affecting block copolymer nanoassemblies: linear block copolymers versus star block copolymers under PISA conditions. *Macromolecules* **2018**, *51*, 5440–5449.
48 Cao, M.; Han, G.; Duan, W.; Zhang, W. Synthesis of multi-arm star thermo-responsive polymers and topology effects on phase transition. *Polym. Chem.* **2018**, *9*, 2625–2633.
49 Zhang, Y.; Guan, T.; Han, G.; Guo, T.; Zhang, W. Star Block Copolymer Nanoassemblies: Block Sequence Is All-Important. *Macromolecules* **2019**, *52*, 718–728.
50 Liu, D.; Chen, Y.; Zhang, L.; Tan, J. Efficient preparation of branched block copolymer assemblies by photoinitiated RAFT self-condensing vinyl dispersion polymerization. *Macromolecules* **2020**, *53*, 9725–9735.
51 Cai, W.; Yang, S.; Zhang, L.; Chen, Y.; Zhang, L.; Tan, J. Efficient synthesis and self-assembly of segmented hyperbranched block copolymers via RAFT-mediated dispersion polymerization using segmented hyperbranched macro-RAFT agents. *Macromolecules* **2022**, *55*, 5775–5787.
52 Liu, D.; Yang, S.; Peng, S.; Chen, Y.; Zhang, L.; Tan, J. Simultaneous synthesis and self-assembly of bottlebrush block copolymers at room temperature *via* photoinitiated RAFT dispersion polymerization. *Macromol. Rapid Commun.* **2022**, *43*, 2100921.
53 Wu, J.; Zhang, L.; Chen, Y.; Tan, J. Linear and star block copolymer nanoparticles prepared by heterogeneous RAFT polymerization using an *ω*,*ω*-heterodifunctional macro-RAFT agent. *ACS Macro Lett.* **2022**, *11*, 910–918.
54 Lin, W.; Jia, S.; Li, Y.; Zhang, L.; Liu, H.; Tan, J. Aqueous RAFT dispersion polymerization mediated by an *ω*,*ω*-macromolecular chain transfer monomer: an efficient approach for amphiphilic branched block copolymers and the assemblies. *ACS Macro Lett.* **2024**, *13*, 1022–1030.
55 Wang, R.; Zhu, W.; Zhang, L.; Sheng, X.; Tan, J. Synthesis of self-assembled star/linear block copolymer blends *via* aqueous RAFT dispersion polymerization. *Chin. J. Chem.* **2024**, *42*, 1606–1614.
56 Xie, G.; Wu, J.; Zhang, L.; Tan, J. Efficient synthesis of *μ*-A(BC)C miktoarm star polymer assemblies *via* aqueous photoinitiated polymerization-induced self-assembly. *Langmuir* **2024**, *40*, 17098–17108.
57 Ferji, K.; Venturini, P.; Cleymand, F.; Chassenieux, C.; Six, J. L. *In situ* glyco-nanostructure formulation *via* photo-polymerization induced self-assembly. *Polym. Chem.* **2018**, *9*, 2868–2872.
58 Georgiou, P. G.; Kontopoulou, I.; Congdon, T. R.; Gibson, M. I. Ice recrystallisation inhibiting polymer nano-objects *via* saline-tolerant polymerisation-induced self-assembly. *Mater. Horiz.* **2020**, *7*, 1883–1887.
59 Zeng, R.; Chen, Y.; Zhang, L.; Tan, J. R-RAFT or Z-RAFT? Well-defined star block copolymer nano-objects prepared by RAFT-mediated polymerization-induced self-assembly. *Macromolecules* **2020**, *53*, 1557–1566.
60 Shanmugam, S.; Cuthbert, J.; Kowalewski, T.; Boyer, C.; Matyjaszewski, K. Catalyst-free selective photoactivation of RAFT polymerization: a facile route for preparation of comblike and bottlebrush polymers. *Macromolecules* **2018**, *51*, 7776–7784.
61 Chen, K.; Hu, X.; Zhu, N.; Guo, K. Design, synthesis, and self-assembly of Janus bottlebrush polymers. *Macromol. Rapid Commun.* **2020**, *41*, 2000357.
62 Yang, S.; Zhang, L.; Chen, Y.; Tan, J. Combining green light-activated photoiniferter RAFT polymerization and RAFT dispersion polymerization for graft copolymer assemblies. *Macromolecules* **2022**, *55*, 8472–8484.
63 Gody, G.; Zetterlund, P. B.; Perrier, S.; Harrisson, S. The limits of precision monomer placement in chain growth polymerization. *Nat. Commun.* **2016**, *7*, 10514.
64 Doncom, K. E. B.; Blackman, L. D.; Wright, D. B.; Gibson, M. I.; O'Reilly, R. K. Dispersity effects in polymer self-assemblies: a matter of hierarchical control. *Chem. Soc. Rev.* **2017**, *46*, 4119–4134.
65 Gao, C.; Li, S.; Li, Q.; Shi, P.; Shah, S. A.; Zhang, W. Dispersion RAFT polymerization: comparison between the monofunctional and bifunctional macromolecular RAFT agents. *Polym. Chem.* **2014**, *5*, 6957–6966.
66 Blanazs, A.; Madsen, J.; Battaglia, G.; Ryan, A. J.; Armes, S. P. Mechanistic insights for block copolymer morphologies: how do worms form vesicles. *J. Am. Chem. Soc.* **2011**, *133*, 16581–16587.
67 Tan, J.; Xu, Q.; Li, X.; He, J.; Zhang, Y.; Dai, X.; Yu, L.; Zeng, R.; Zhang, L. Enzyme-PISA: an efficient method for preparing well-defined polymer nano-objects under mild conditions. *Macromol. Rapid Commun.* **2018**, *39*, 1700871.
68 Liu, D.; Cai, W.; Zhang, L.; Boyer, C.; Tan, J. Efficient photoinitiated polymerization-induced self-assembly with oxygen tolerance through dual-wavelength type I photoinitiation and photoinduced deoxygenation. *Macromolecules* **2020**, *53*, 1212–1223.

https://doi.org/10.1007/s10118-025-3275-0